Journal of The Electrochemical Society, **157** (11) B1679-B1685 (2010)
0013-4651/2010/157(11)/B1679/7/$28.00 © The Electrochemical Society

Mesoporous Carbon and Poly(3,4-ethylenedioxythiophene) Composite as Catalyst Support for Polymer Electrolyte Fuel Cells

K. K. Tintula,[a] A. K. Sahu,[a] A. Shahid,[b] S. Pitchumani,[a] P. Sridhar,[a,*] and A. K. Shukla[c,*,z]

[a]*CSIR-CECRI-Madras Unit, CSIR Madras Complex, Taramani, Chennai 600 113, India*
[b]*CSIR-Central Electrochemical Research Institute (CECRI), Karaikudi 600 036, India*
[c]*Solid State and Structural Chemistry Unit, Indian Institute of Science, Bangalore 560 012, India*

In situ polymerization of 3,4-ethylenedioxythiophene with sol–gel-derived mesoporous carbon (MC) leading to a new composite and its subsequent impregnation with Pt nanoparticles for application in polymer electrolyte fuel cells (PEFCs) is reported. The composite exhibits good dispersion and utilization of platinum nanoparticles akin to other commonly used microporous carbon materials, such as carbon black. Pt-supported MC–poly(3,4-ethylenedioxythiophene) (PEDOT) composite also exhibits promising electrocatalytic activity toward oxygen reduction reaction, which is central to PEFCs. The PEFC with Pt-loaded MC-PEDOT support exhibits 75% of enhancement in its power density in relation to the PEFC with Pt-loaded pristine MC support while operating under identical conditions. It is conjectured that Pt-supported MC–PEDOT composite ameliorates PEFC performance/durability on repetitive potential cycling.
 [DOI: 10.1149/1.3486172]

Manuscript submitted June 25, 2010; revised manuscript received August 9, 2010. Published September 23, 2010.

Commercial viability of the polymer electrolyte fuel cells (PEFCs) requires almost an order of magnitude reduction in Pt usage with improved performance and durability.[1-5] The U.S. Department of Energy has set targets for electrocatalyst performance for the year 2010 at a mass activity of 0.44 $A/mg_{(Pt)}$ as compared against the current value of 0.28 $A/mg_{(Pt)}$ and an electrochemical surface area (ESA) $<40\%$ after accelerated aging. In the literature,[6-16] efforts are being expended to improve the performance and durability of electrocatalysts in PEFCs by alloying Pt with transition metals, such as Ru, Ir, Co, Ti, Zr, Sn, etc., heat-treatment of Pt-based alloys, preparation of core–shell catalysts, dealloying Pt metal alloys, and adapting conducting polymers for developing a durable porous catalyst support with a suitable surface area.

A fuel cell catalyst support should have a large surface area with adequate surface functionalities for finely dispersing catalytic metal particles, high electrical conductivity for providing electrical pathways, and highly developed mesoporosity to facilitate diffusion of reactants and products in conjunction with high electrochemical stability during long-term operation.[17,18] Carbon supports, such as carbon black and activated carbon that are being currently used, usually exhibit a large surface area but their pore structures are primarily microporous[19] with pore sizes <2 nm, which makes the microporous structures incompatible for transporting the reactants; besides, catalyst particles get buried in the micropores making them inaccessible to fuel[20,21] and hence to the overall electrochemical process. Furthermore, these carbon supports, being prone to corrosion caused by electrochemical oxidation during repetitive PEFC cycling, limit its operational life.[22-24]

To address the aforesaid issues, electrically conducting graphitic carbon nanomaterials, namely, carbon nanotubes, carbon nanofibers, and graphitic porous carbon, have been widely employed as potential carbon supports.[25-32] However, synthesis of a high surface area graphitic carbon is challenging, and exploration of a cost-effective method for their large-scale production has been eluding.

Mesoporous carbon (MC) is a functionally superior material with excellent chemical/thermal stability desired for catalysis.[33-41] MC materials with regular arrays of uniform mesopores are highly attractive from the viewpoint of pore structure, pore volume, and pore size distribution (PSD) desired to facilitate mass transport for maximum Pt utilization that enables encountering problems inherent with microporous carbon supports.[42-47] To improve the performance of a catalyst, modifications in both surface chemistry and pore structure of MC are required. Carbon is usually subjected to post-treatments including oxidation, polymer coating, and grafting for increasing the number of surface functional groups.[48-51] In many cases, acidic groups, such as nitric acid, sulfuric acid, phosphoric acid, alone or in combination, are used for functionalizing MC. This provides sufficient binding sites for anchoring Pt nanoparticles and allows high metal loading onto the carbon support.[38,48,52] However, functionalization with aforesaid acid treatments affects the pore structure of MC with substantial reduction in their surface area. Such harsh chemical oxidation methods also reduce the electrical conductivity and corrosion resistance of MC. Therefore, it is highly desirable to develop mild surface functionalization methods to introduce high density and homogenous surface-functional groups with limited structural damage to MCs.

Conducting polymers have received much attention as an alternative catalyst support because of their attractive accessible surface area, low resistance, high stability and tolerance to CO poisoning.[53] Conducting polymers possess electronic conductivity between 10^{-6} and 10^{3} S/cm and have found wide applications in sensors, electrochemical actuators, corrosion inhibitors, and polymeric batteries.[54-58] Metal nanoparticle impregnation on a conducting polymer matrix facilitates flow of electronic charges between them during the electrochemical reaction. But due to low surface area and nonporous structure of conducting polymers, the dispersion of Pt particles and their utilization in the matrix remains limited. The combination of an MC with a conducting polymer, such as polypyrrole and poly(3,4-ethylenedioxythiophene) (PEDOT) may help mitigate the aforesaid disadvantages due to the robust pore structure and high surface area of MCs in conjunction with the good corrosion resistance and catalytic activity of conducting polymers.[59-61] Besides, such a combination appears to be most adequate as catalyst support for fuel cell applications where the Pt nanoparticles can be optimally dispersed for maximizing Pt utilization.

Among the conducting polymers, characteristics such as high chemical and thermal stability[62] and high electrical conductivity[63] of PEDOT make it attractive for use as support material for fuel cell catalysts.[64] The electron-conducting property of PEDOT remains nearly unaffected even after prolonged aging in harsh environmental conditions owing to favorable ring geometry and presence of electron donating atoms at the 3,4 positions, which help stabilize the positive charge in the polymer backbone.[65] In this study, we report surface modification of an MC with PEDOT, through an in situ polymerization reaction leading to formation of an MC–PEDOT composite. Selective adsorption of 3,4-ethylenedioxythiophene

* Electrochemical Society Active Member.
z E-mail: akshukla2006@gmail.com

(EDOT) on the surface of the MC and its subsequent polymerization helps form an MC–PEDOT composite with little effect on the pore structure of MC. Pt particles are impregnated onto the MC–PEDOT composite using formaldehyde reduction method. A PEFC operating with a Pt/(MC–PEDOT) composite catalyst exhibits higher performance toward oxygen reduction reaction (ORR) with high durability in relation to the PEFC with pristine Pt/MC or Pt/Vulcan XC-72R catalyst.

Experimental

Materials.— EDOT and Pluronic-F127 were obtained from Sigma-Aldrich, whereas chloroplatinic acid (Alfa Aesar), phloroglucinol dihydrate (99%), sodium salt of polystyrene sulfonic acid, ammonium persulphate, and methanol were procured from Acros organics. Formaldehyde (37–41%), hydrochloric acid (37%), and absolute ethanol were procured from Merck, Germany. Vulcan XC-72R carbon was obtained from Cabot Corporation. All the chemicals were used as received. Deionized (DI) water (18.4 MΩ cm) used for the experiments was produced by a Millipore system.

Synthesis of the catalyst support material.— MC with a specific surface area of 370 m^2/g, average pore diameter of 6.7 nm, and average pore volume of 0.45 cm^3/g was synthesized by a coassembly route without usage of any hard template, as described elsewhere.[66] MC was thermally treated at 100°C in a vacuum oven to remove the physically adsorbed water. Chemical polymerization of EDOT on the surface of MC was performed with ammonium persulfate as an oxidant similar to the process reported by Wang et al.[67] The required amount of MC was immersed in 12 M aqueous methanol solution with varying EDOT contents in acidic medium and stirred for 1 h. To the above admixture, aqueous 0.05 M solution of ammonium persulfate was added drop wise with mechanical stirring between 0 and 5°C followed by further stirring for 4 h. The product was filtered and washed copiously with DI water and methanol. The resulting MC–PEDOT composite was dried under vacuum at 80°C for 12 h. The amount of PEDOT in the MC–PEDOT composite was varied as 20, 30, and 50 wt %.

Catalyst preparation.— Both MC and MC–PEDOT composite supported Pt catalysts were prepared by the formaldehyde reduction method. In brief, the support material was first suspended in an appropriate amount of chloroplatinic acid in aqueous medium and pH of the mixed solution was adjusted to 12 by using an aqueos 0.5 M NaOH solution. Subsequently, formaldehyde was added drop wise to the slurry. The mixture was refluxed in an oil bath at 90°C for 3 h. An aqueous solution of $NaNO_3$ was added to the above solution as a sedimentation promoter. The above mixtures were filtered and washed with copious amount of water followed by drying under vacuum at 80°C for 12 h.

Physicochemical characterization.— The presence of a conducting polymer on the surface of MC was confirmed by a Fourier transform infrared (FTIR) spectroscope (Thermo Nicolet, model Nexus 670) using KBr pellet method. The thermal stability of MC and MC–PEDOT composites were studied using an SDT Q600 V8.2 TGA instrument between 30 and 700°C at a heating rate of 10°C/min under N_2 atmosphere. Textural and surface properties of carbon supports were characterized by N_2 physisorption and temperature-programmed desorption, respectively. Nitrogen-sorption isotherms were obtained at 77 K using a Micromeritics ASAP 2020. Total surface areas and pore volumes for the samples were determined by Brunauer–Emmett–Teller (BET) and the single-point methods, respectively. PSD curves were obtained by Barrett–Joyner–Halenda (BJH) method, and the position of the maximum in the PSD was used as the average pore diameter. Powder X-ray diffraction (XRD) patterns for supported catalyst samples were obtained on a Philips PanAnalytical X-ray diffractometer employing Cu Kα radiation of wavelength 1.54 Å. Transmission electron microscope (TEM) images for determining structural changes and the Pt particle distribution in the supporting material were obtained using a 200 KV Tecnai-20 G2. For these measurements, the samples were suspended in acetone with ultrasonic dispersion for 3 min. Subsequently, a drop of the suspension was deposited on a carbon-coated copper grid and allowed for drying. TEM images for the samples were recorded with a bottom-mounted MultiScan charge-coupled device camera (model 794, Gatan) using low dose conditions.

Electrochemical measurements.— Electrochemical tests on the catalysts were performed with a rotating disk electrode (RDE) apparatus (Eco Chemie BV) at room temperature (~25°C). A glassy carbon disk (geometric area of 0.071 cm^2) was used as a substrate for the catalyst. A catalyst suspension was obtained by adding 6.3 mg of catalyst to 10 mL water mixed with a 30 wt % Nafion solution (DuPont) followed by ultrasonication for 30 min. A 10 μL aliquot of the dispersed suspension was pipetted onto the substrate to obtain a Pt loading of 35.5 $\mu g/cm^2$. Pt wire and saturated calomel electrode (SCE) were used as counter and reference electrodes, respectively. Linear sweep voltammetry for ORR activity measurements was performed using RDE in aqueous 0.5 M $HClO_4$ saturated with O_2 at a scan rate of 1 mV/s with a rotation speed of 1600 rpm. To test the electrochemical stability of the catalyst, 500 cycles were performed in aqueous 0.5 M $HClO_4$ solution at a scan rate of 50 mV/s between −0.25 and 0.8 V vs SCE.

Fabrication of MEA.— 15 wt % teflonized Toray TGP-H-120 carbon paper of 0.37 mm thick was used as the backing layer. To prepare a gas diffusion layer (GDL), Vulcan XC-72R carbon was suspended in cyclohexane and agitated in an ultrasonic water bath for 30 min. To this solution, 15 wt % poly(tetrafluroethene) suspension in 2 mL ammonia was added with continuous agitation to form a slurry to coat on the backing layer uniformly until the required loading of 1.5 mg/cm^2 was attained. The GDL thus obtained was sintered in a furnace at ~350°C for 30 min. For the reaction layer, prepared catalysts were dispersed separately in isopropyl alcohol and ultrasonicated for 30 min followed by the addition of 30 wt % of Nafion solution; the resultant slurries were ultrasonicated for 1 h and coated onto the GDLs (represented as cathode) until a Pt loading of 0.5 mg cm^{-2} was achieved. For the anode, 40 wt % Pt/C (Johnson Matthey) was used with 7 wt % of Nafion loading. A membrane electrode assembly (MEA) was obtained by sandwiching the pretreated Nafion 1135 membrane between the two electrodes followed by its hot compaction under a pressure of 60 kg/cm^2 at 130°C for 3 min. MEAs were coupled with Teflon gas-sealing gaskets and placed in a single-cell test fixture with a parallel serpentine flow field machined on graphite plates. Gaseous H_2 and gaseous O_2 were fed to the anode and cathode of the PEFC, respectively, through the bubble humidifiers kept at 10°C higher than the cell temperature. The flow rates of both the reactants were kept at 100 mL/min. After equilibration at a cell temperature of 60°C, galvanostatic polarization data were obtained using an LCN100-36 electronic load from Bitrode Corporation. All the MEAs were evaluated in a 4 cm^2 PEFC under atmospheric pressure.

Cyclic voltammograms (CVs) were recorded in fuel cell mode at ~25°C to determine the ESA of catalysts using a potentiostat (Autolab PGSTAT 30) with its reference and counter electrodes connected to the cell anode and its working electrode to the cell cathode. During the experiment, gaseous hydrogen and gaseous nitrogen were fed to the anode and cathode, respectively, at a flow rate of 100 mL/min. Voltammograms were recorded after a run time of 1 h, with the working electrode cycled between 0 and 1 V at a sweep rate of 50 mV/s, to obtain stable and reproducible data.

Results and Discussion

Physicochemical characterization.— FTIR spectra for MC–PEDOT composites are shown in Fig. 1. In the spectra, the peaks at 1340 and 1518 cm^{-1} are due to the C–C and C = C stretching of the thiophene ring, respectively, whereas the peaks at 685, 841, and 975 cm^{-1} represent C–S vibration modes of the thiophene ring

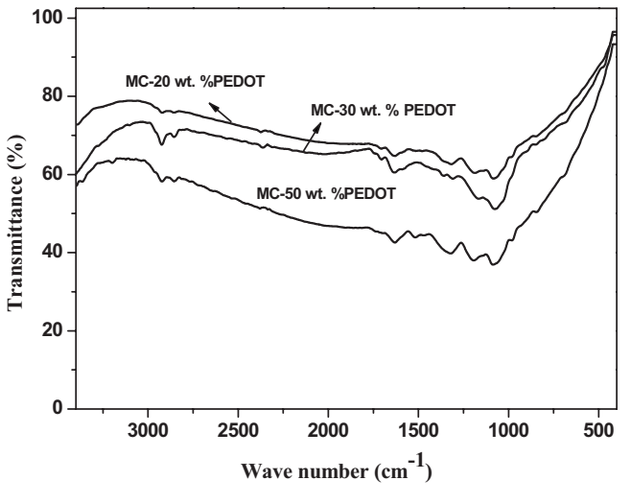

Figure 1. FTIR spectra for MC and MC–PEDOT composites between 500 and 3500 cm^{-1} wavenumber in transmittance mode.

present in composites and the peaks at 1083 and 1198 cm^{-1} are assigned to stretching mode of ethylene dioxy (C–O–C) group of PEDOT.[68] It can be seen that the characteristic peak intensities corresponding to PEDOT increase with increasing PEDOT content.

Thermogravimetric analysis (TGA) curves for pristine MC and MC–PEDOT composites are shown in Fig. 2. The first weight loss between 100 and 120°C is observed due to the removal of physisorbed water (residual humidity). The weight loss is higher for the MC–PEDOT composite indicating its higher hydrophilic nature in relation to pristine MC. The second weight loss for the MC–PEDOT composite in the temperature range between 120 and 450°C is assigned to the thermal decomposition of PEDOT. The amount of PEDOT loaded on MC is determined using the residual weight difference between the MC–PEDOT composite and the pristine MC from TGA traces at 700°C. The residual weight percentage at 700°C is 64.2% for pristine MC, whereas the residual weight percentages for 20, 30, and 50 wt % MC–PEDOT composites are 45.2, 35.2, and 15.5%, respectively. The amounts of PEDOT are calculated as reported[60] and are found to be 19, 29, and 48.6% for MC–20 wt % PEDOT, MC–30 wt % PEDOT, and MC–50 wt % PEDOT, respectively.

The textural effects of PEDOT polymerization on MC are illustrated by N_2 sorption isotherms and PSD analysis shown in Fig. 3a and b, respectively. Both MC and MC–PEDOT composites exhibit

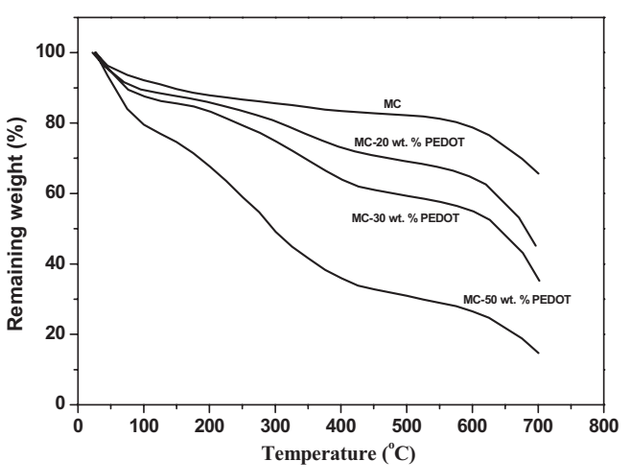

Figure 2. TGA for MC and MC–PEDOT composites.

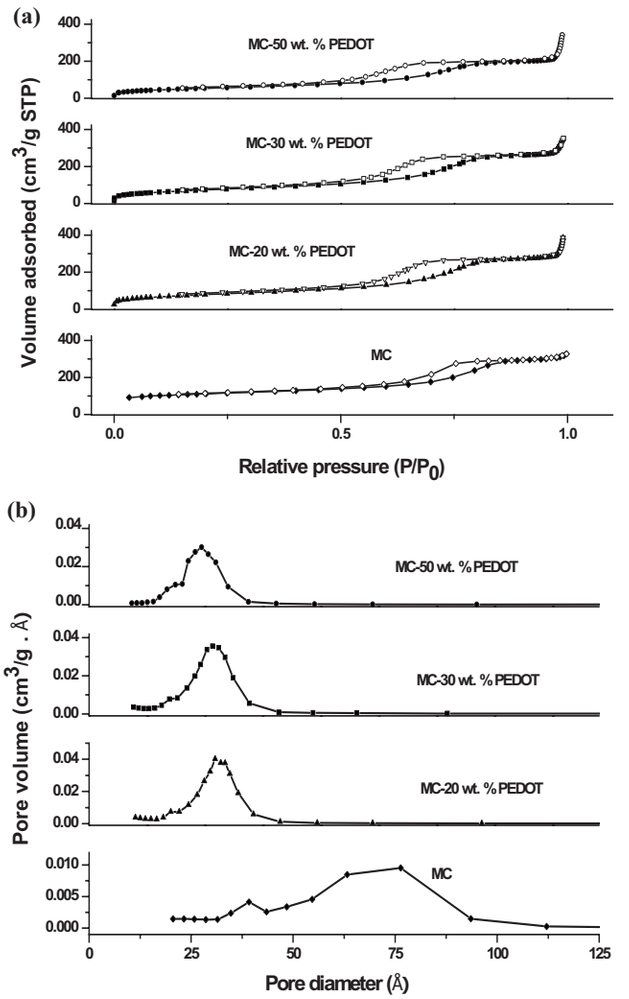

Figure 3. (a) Nitrogen sorption isotherms for MC and MC–PEDOT composites and (b) corresponding PSD for MC and MC–PEDOT composites.

type IV isotherm with a pronounced hysteresis loop in conjunction with a sharp capillary condensation at a high relative pressure, indicating the presence of mesopores, whereas type II isotherm is typically observed for nonporous and macroporous materials.[66,69] The respective BET surface areas for pristine MC, MC–20 wt % PEDOT, MC–30 wt % PEDOT, and MC–50 wt % PEDOT composites are found to be 370, 278, 262, and 118 m^2/g (see Table I). The pore sizes and pore volumes for composite supports are lower in relation to pristine MC. The decrease in surface area, pore size, and pore volume for MC–PEDOT composites might be due to surface coverage of MC by PEDOT during polymerization process.[18] For further insight into the internal pore structure of MC and MC–PEDOT composites, TEM analysis is carried out as shown in Fig. 4. Only a little structural variation with decrease in pore size is observed for the

Table I. Physical parameters for MC and MC–PEDOT composites.

Composites	BET surface area (m^2/g)	BJH pore size (nm)	Pore volume (cm^3/g)
MC	370	6.7	0.45
MC–20 wt % PEDOT	278	3.9	0.40
MC–30 wt % PEDOT	262	3.6	0.37
MC–50 wt % PEDOT	118	3.1	0.26

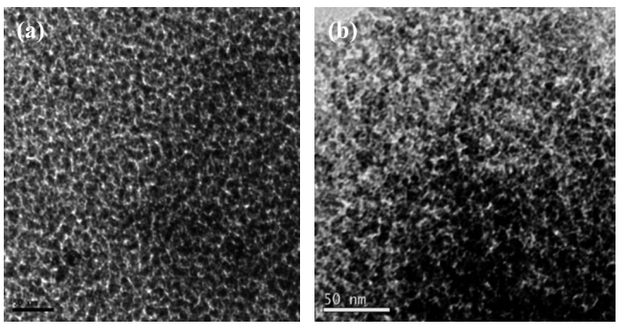

Figure 4. Representative TEM images for (a) pristine MC and (b) MC–30 wt % PEDOT composite (scale bar = 50 nm).

MC–PEDOT composites in relation to pristine MC. The monomer easily penetrates and adsorbs in large pores in MC, which on subsequent polymerization leads to narrow PSD for MC–PEDOT composites in relation to pristine MC. This further supports that the polymerization of PEDOT on MC only has a marginal effect on the microstructural changes in agreement with the N_2 sorption isotherm and PSD curves, as shown in Fig. 3.

To explore the feasibility of MC–PEDOT composites as a catalyst support for fuel cells, about 40 wt % of Pt is loaded on to the supporting material. Powder XRD patterns for Pt loaded onto MC, MC–PEDOT composites, and Vulcan XC-72R are shown in Fig. 5. For all the samples, the characteristic peaks at 39.96, 46.22, and 67.59° assigned to the (111), (210), and (220) reflections of crystalline Pt characteristic of face-centered cubic phase of Pt. The average Pt particle size is calculated from Scherrer's equation based on the Pt(111) diffraction peak. The average particle size values for Pt/MC–20 wt % PEDOT, Pt/MC–30 wt % PEDOT, and Pt/MC–50 wt % PEDOT as obtained from the Scherrer equation are 3.6, 3.4, and 6.2 nm, respectively, whereas the particle size for Pt/Vulcan XC-72R is 4.2 nm. In relation to Pt/MC, Pt/MC–PEDOT composites comprise smaller Pt crystallites suggesting PEDOT to have more number of available surface groups for anchoring Pt particles. This in turn helps increase dispersion of Pt particles in the composites. There is not much difference in Pt particle size with varying PEDOT content in the MC–PEDOT composites.

The morphologies of Pt particles in MC and MC–PEDOT composites are analyzed by TEM images shown in Fig. 6. Electron diffraction peaks shown in the inset of Fig. 6 confirms the polycrystalline nature of Pt nanoparticles. The ring pattern in diffraction micrographs once again confirms the particle size to be in the nanoregime. The ring pattern is indexed and the diffraction pattern matches with cubic Pt phase (PDF 040802). Pt particles are in the size range of 6–8 nm with agglomeration in some region in the case of Pt impregnated in pristine MC. However, spherical Pt particles are widespread and homogeneously dispersed in the MC–PEDOT composites. Surface polymerization of PEDOT on MC increases surface binding sites, mitigates the formation of Pt aggregates, improves the dispersion of metal nanoparticles, and reduces the average size of deposited metal nanoparticles. Pt particles of about 2–3 nm are observed in the composites comprising MC–20 wt % PEDOT and MC–30 wt % PEDOT, whereas Pt particles of about 4–5 nm are observed for the MC–50 wt % PEDOT composite. The population density of Pt particles increases with PEDOT content in the composite due to availability of more number of anchoring sites. An increase in Pt particle size in MC–50 wt % PEDOT composite is due to a decrease in the surface area of the composite as observed from the N_2 sorption isotherm leading to particle growth in the composite.

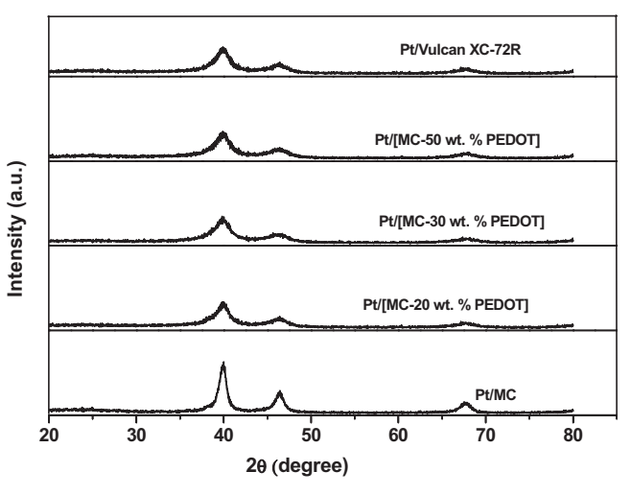

Figure 5. XRD patterns of Pt/MC and Pt/MC–PEDOT composites and Pt/Vulcan XC-72R.

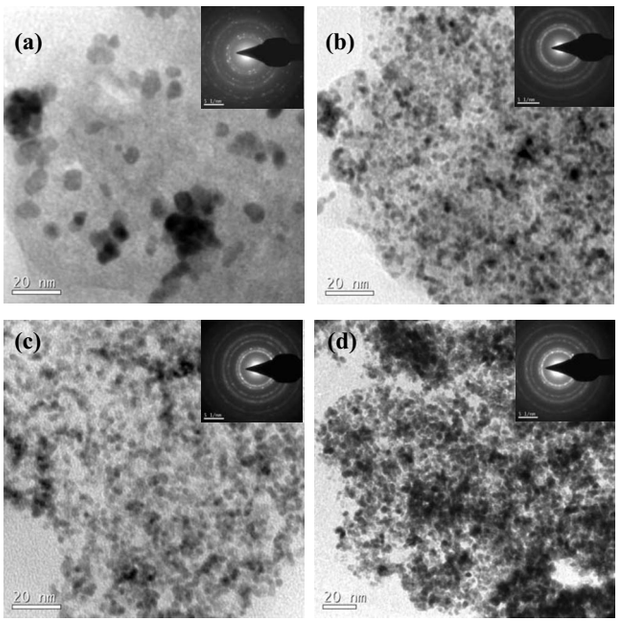

Figure 6. TEM images for (a) Pt/MC, (b) Pt/MC–20 wt % PEDOT, (c) Pt/MC–30 wt % PEDOT, and (d) Pt/MC–50 wt % PEDOT.

Cyclic voltammetry.— CVs for catalysts measured in fuel cell mode are presented in Fig. 7. All catalysts exhibit similar oxidation and reduction peaks, with slightly different shapes. Two to three peaks are observed between 0.05 and 0.4 V, where adsorbed hydrogen is oxidatively desorbed. The change in shape for oxidation peaks observed may be attributed to the development of different crystalline facets on the supporting materials. In the reduction scan, the CVs show a peak between 0.6 and 0.8 V corresponding to the reduction of surface oxide on Pt nanoparticles. The ESA for the as-prepared catalysts are obtained by integrating the total charge corresponding to the adsorption/desorption peak of hydrogen followed by normalizing the scan rate, Pt loading, and the charge value of 210 $\mu C/cm^2$ for the Pt surface, and the values are given in Table II. The hydrogen adsorption/desorption charge is 94.5 mC/cm^2 after subtracting the double-layer charge amounting to 35 mC/cm^2 for Pt/MC–PEDOT (30 wt %). Pt/MC has the lowest ESA due to the poor distribution of Pt particles, as shown in Fig. 6a. By contrast, Pt particles supported on composites have a large ESA in relation to MC-supported Pt. The increase in ESA for MC–PEDOT composites

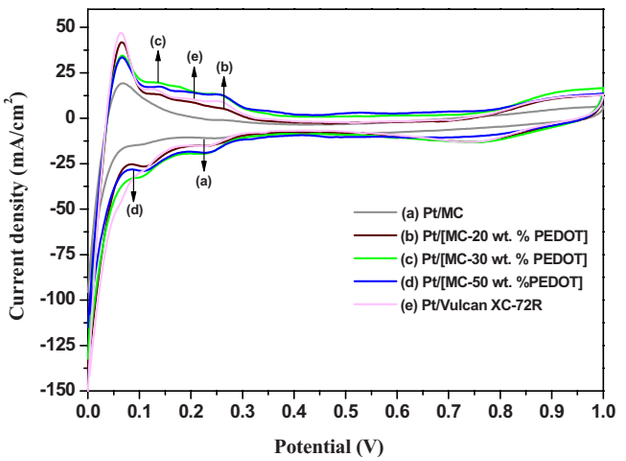

Figure 7. (Color online) CVs for Pt/MC, Pt/MC–20 wt % PEDOT, Pt/MC–30 wt % PEDOT, Pt/MC–50 wt % PEDOT, and Pt/Vulcan XC-72R recorded at 25°C in a single cell with H_2 and N_2 streams at the anode and cathode, respectively (scan rate = 50 mV s^{-1}).

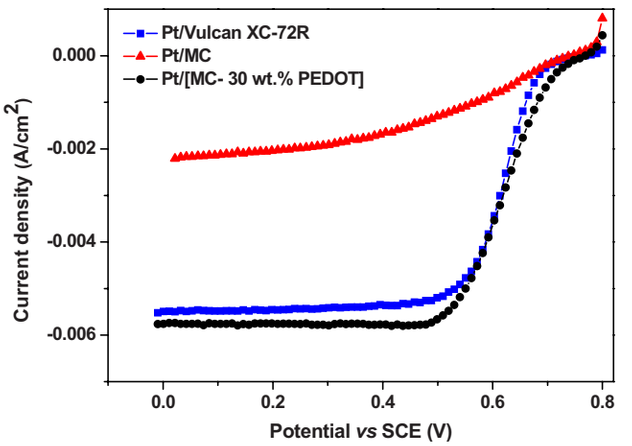

Figure 8. (Color online) Linear sweep voltammograms for Pt/MC, Pt/MC–30 wt % PEDOT and Pt/Vulcan XC-72R supported on a glassy carbon electrode at 1600 rpm in O_2-saturated aqueous 0.5 M $HClO_4$.

in relation to MC is due to the availability of more number of surface groups to anchor on Pt particles in presence of PEDOT resulting in uniform distribution of nanoparticles.

ORR activity.— Electrochemical activities for catalysts are investigated using RDE in acidic solution at room temperature to ascertain the catalytic activity for oxygen reduction as depicted in Fig. 8. Pt on MC–PEDOT is superior toward ORR in relation to pristine MC. The corresponding onset potential for Pt/MC–30 wt % PEDOT is greater than those for Pt/MC and Pt/Vulcan XC-72R. PEDOT exhibits electrocatalytic activity toward ORR.[59] From the same experimental data, the mass activities of the catalysts are obtained by calculating i_k, the mass-transport-free kinetic current normalized to the Pt loading.[70] At 0.65V vs SCE, the mass activities for Pt/MC, Pt/MC–30 wt % PEDOT, and Pt/Vulcan XC-72R are found to be 0.019, 0.08, and 0.051 A/$mg_{(Pt)}$, respectively, at room temperature with a sweep rate of 1 mV/s in O_2-saturated 0.5 M aqueous $HClO_4$ at 1600 rpm. In the present study, Pt supported on an MC–PEDOT composite exhibits improved activity due to the presence of PEDOT, which acts as an active electron exchanger during the electrochemical reaction and results in higher oxygen reduction current for Pt particles impregnated in MC–PEDOT composite in relation to Pt particles supported on pristine MC, suggesting a considerable increase in the catalytic activity for the former.

Fuel cell test.— Figure 9 shows the performance data for PEFCs with MEAs of all the catalysts tested under identical experimental conditions. Because Pt/Vulcan XC-72 R is used as the anode for all MEAs, variation in performance is attributed only due to ORR on the cathode catalyst. As PEDOT content increases from 20 to 30 wt % in the MC–PEDOT composites, the PEFC performance also increases. However, a further increase in the PEDOT content deteriorates the PEFC performance due to significant structural changes. As shown in the TEM image, the dispersion of Pt nanoparticle is improved in the MC–PEDOT composites that increases ESA and hence the PEFC performance. From the textural features and the PEFC polarization data, it is surmised that a balance between the surface area and dispersion of Pt particles in the composites is mandatory. In this study, the optimum PEDOT content in the MC–PEDOT composites is 30 wt % for the maximum performance for PEFC. In general, a porous structure facilitates more Pt particles for participating in electrochemical reaction that improves the PEFC perfor-

Table II. Effect of potential cycling on ESA of the catalysts employed in this study.

	ESA (m^2/g)			
Catalysts	Initial	100th cycle	300th cycle	500th cycle
Pt/MC	36.4	34.2	31.3	30.2
Pt/(MC–20 wt % PEDOT)	85.7	81.4	73.7	70.3
Pt/(MC–30 wt % PEDOT)	90	83.7	79.2	76.5
Pt/(MC–50 wt % PEDOT)	81.4	77.3	72.5	70
Pt/Vulcan XC-72R	89	85.3	72	66.7

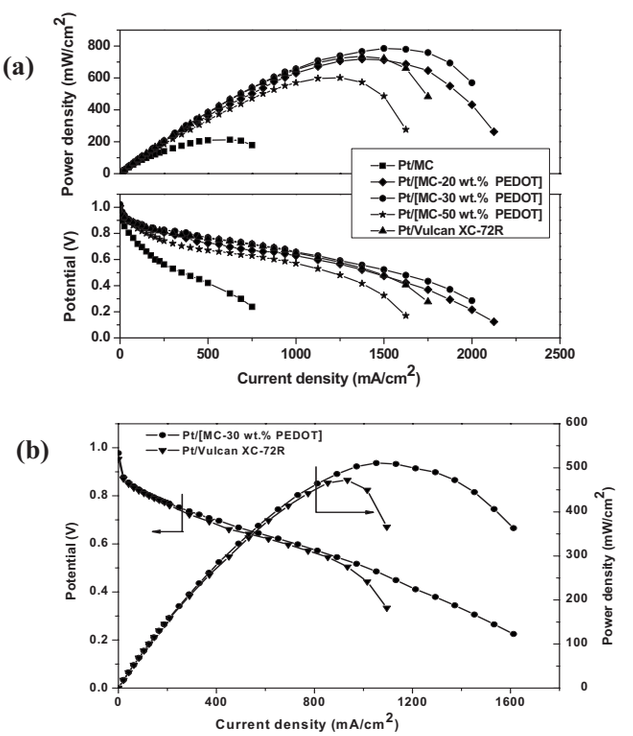

Figure 9. Performance curves for (a) H_2–O_2 PEFC comprising Pt/MC, Pt/MC–PEDOT composites and Pt/Vulcan XC-72R as cathode catalysts and (b) H_2 air PEFC comprising Pt/MC–30 wt % PEDOT composites and Pt/Vulcan XC-72R as cathode catalysts.

Table III. Electrode kinetic parameters for PEFCs with MC, MC–PEDOT composites, and Vulcan XC-72R as catalyst supports.

Catalysts	E_0 (V)	$i_{(0.9\ V)}$ (A/mg_{Pt})	$i_{(0.9\ V)}$ ($\mu A/cm^2_{Pt}$)	$i_{(0.9\ V)}$ (mA/cm^2_{geo})	b (mV/dec)
Pt/MC	0.98	0.024	65.9	12.3	257
Pt/(MC–20 wt % PEDOT)	1.01	0.102	119	51	73.3
Pt/(MC–30 wt % PEDOT)	1.02	0.119	132	59.8	63
Pt/(MC–50 wt % PEDOT)	0.99	0.079	97	39.7	86.4
Pt/Vulcan XC-72R	0.97	0.1	112	50	68

mance. Besides, the porous structure allows free flow of oxidant as well as easy removal of product water extending the operation of PEFC to high load current densities, as shown in Fig. 9a. By contrast, the PEFC employing Pt/Vulcan XC-72R shows poor mass transfer primarily due to the presence of micropores in the carbon support. For further confirmation, the PEFCs comprising Pt/Vulcan XC-72R and Pt/MC–30 wt % PEDOT are operated with H_2 air under atmospheric pressure, as shown in Fig. 9b. The PEFC with MC–30 wt % PEDOT shows better performance at high load current densities owing to improved reactant gas distribution and removal of product water.[66] The peak power density of 510 mW/cm^2 at a load current density of 1050 mA/cm^2 is achieved for the PEFC with MC–30 wt % PEDOT as compared to the peak power density of 470 mW/cm^2 at a load current density of 930 mA/cm^2 for the PEFC with Vulcan XC-72R.

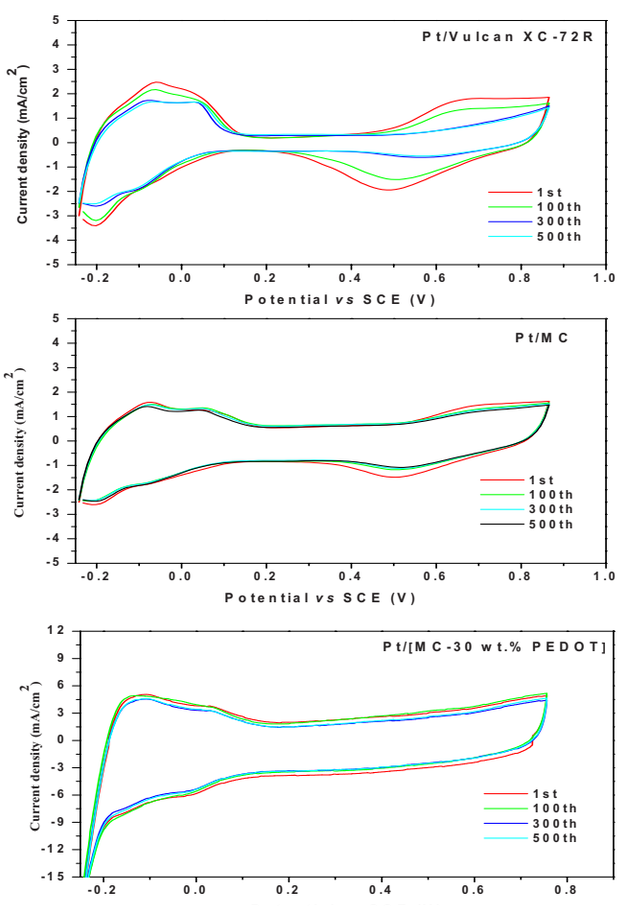

Figure 10. (Color online) CVs for Pt/MC, Pt/MC–30 wt % PEDOT and Pt/Vulcan XC-72R in N_2-purged 0.5 M aqueous $HClO_4$ at a scan rate of 50 mV s^{-1}.

The cell potential (E) vs current density (i) data for different catalysts in H_2–O_2 PEFCs are analyzed by Eq. 1

$$E = E_0 - b \log i - R_i i \quad [1]$$

assuming the mass-transport limitations to be negligible at low load current densities and considering hydrogen oxidation reaction to be fast.

In Eq. 1, $E_0 = E_r + b \log i_0$, where E_r is the thermodynamic reversible potential for fuel cell reaction, i_0 and b are exchange current density and Tafel slope, and R_i is the differential resistance of the cell. The value E_0 is the cell potential at 1 mA/cm^2. In the present analysis, i_0 is replaced with $i_{0.9\ V}$, i.e., current density at a cell potential of 0.9 V because a slight variation in Tafel slope could yield anomalous values for i_0.[71,72] The electrode kinetic parameters are summarized in Table III. The values of E_0 and $i_{0.9\ V}$ are superior for Pt-impregnated MC–30 wt % PEDOT indicating good catalytic activity in agreement with the results obtained from ORR studies. For 20–30 wt % PEDOT in MC–PEDOT composites, the mass activity values are higher compared to 50 wt % loading of PEDOT on MC. The decrease in Tafel slope for the Pt-impregnated MC–30 wt% PEDOT shows an active ORR in comparison to Pt on Vulcan XC-72R.

Durability.— Repeated potentiodynamic cycling between the hydrogen adsorption and the oxide formation potentials can change the ESA of the catalyst. The effect of cycling on the CVs of Pt/Vulcan XC-72R, Pt/MC, and Pt/MC–30 wt% PEDOT composite is depicted in Fig. 10. The current–potential response shows that cycling leads to the proportional decrease in ESA due to increase in Pt particle size by dissolution/redeposition/surface migration resulting in aggregation of Pt particles.[73] The ESA values are culled from the cyclic voltammetric curves and are presented in Table II. From the data, it is seen that the ESA for all catalysts decreases with potential cycling. However, in case of Pt supported onto MC and MC–PEDOT composites, only a marginal decrease in ESA is observed. The loss of ESA for Pt/Vulcan XC-72R is ~25%, whereas the loss of ESA for Pt/MC and Pt/MC–30 wt % PEDOT is ~18 and ~15%, respectively. By contrast, the loss in ESA for Vulcan XC-72R is quite substantial in relation to MC–PEDOT. Clearly, the high electrochemical stability of PEDOT and the robust porous nature of MC provide stability under repetitive potential cycling.

Conclusion

The study reports in situ polymerization of EDOT with sol–gel-derived MC leading to a novel porous catalyst support of optimized composition and the process for insertion of Pt nanoparticles. Homogeneous dispersion of 2–3 nm Pt particles in the composite improves electrocatalytic activity toward ORR leading to enhanced PEFC performance and durability on repetitive potential cycling.

Acknowledgment

Financial support from CSIR, New Delhi is gratefully acknowledged.

Central Electrochemical Research Institute assisted in meeting the publication costs of this article.

References

1. R. Borup, J. Meyers, B. Pivovar, Y. S. Kim, R. Mukundan, N. Garland, D. Myers, M. Wilson, F. Garzon, D. Wood, et al., *Chem. Rev. (Washington, D.C.)*, **107**, 3904 (2007).
2. Y. Shao, G. Yin, and Y. Gao, *J. Power Sources*, **171**, 558 (2007).
3. L. R. Jordan, A. K. Shukla, T. Behrsing, N. R. Avery, B. C. Muddle, and M. Forsyth, *J. Power Sources*, **86**, 250 (2000).
4. Y. Shao-Horn, W. C. Sheng, S. Chen, P. J. Ferreira, E. F. Holby, and D. Morgan, *Top. Catal.*, **46**, 285 (2007).
5. Y. Shao, J. Liu, Y. Wang, and Y. Lin, *J. Mater. Chem.*, **19**, 46 (2009).
6. S. Mukerjee and S. Srinivasan, *J. Electroanal. Chem.*, **357**, 201 (1993).
7. A. K. Shukla, M. Neergat, P. Bera, V. Jayaram, and M. S. Hegde, *J. Electroanal. Chem.*, **504**, 111 (2001).
8. H. R. Colón-Mercado, H. Kim, and B. N. Popov, *Electrochem. Commun.*, **6**, 795 (2004).
9. H. R. Colón-Mercado and B. N. Popov, *J. Power Sources*, **155**, 253 (2006).
10. K. Okaya, H. Yano, H. Uchida, and M. Watanabe, *ACS Appl. Mater. Interfaces*, **2**, 888 (2010).
11. Z. Liu, X. Y. Ling, X. Su, and J. Y. Lee, *J. Phys. Chem. B*, **108**, 8234 (2004).
12. S. Koh and P. Strasser, *J. Electrochem. Soc.*, **157**, B585 (2010).
13. P. Strasser, S. Koh, and J. Greeley, *Phys. Chem. Chem. Phys.*, **10**, 3670 (2008).
14. Z. D. Wei, Y. C. Feng, L. Li, M. J. Liao, Y. Fu, C. X. Sun, Z. G. Shao, and P. K. Shen, *J. Power Sources*, **180**, 84 (2008).
15. J. X. Wang, H. Inada, L. Wu, Y. Zhu, Y. M. Choi, P. Liu, W. P. Zhou, and R. R. Adzic, *J. Am. Chem. Soc.*, **131**, 17298 (2009).
16. Z. Qi, J. Shan, and P. G. Pickup, ACS Symposium Series, Vol. 832, J. F. b. Rubinson and H. B. Mark, Editors, American Chemical Society, p. 166 (2002).
17. A. L. Dicks, *J. Power Sources*, **156**, 128 (2006).
18. H. Chang, S. H. Joo, and C. Pak, *J. Mater. Chem.*, **17**, 3078 (2007).
19. E. Antolini, *Appl. Catal., B*, **88**, 1 (2008).
20. S. D. Thompson, L. R. Jordan, and M. Forsyth, *Electrochim. Acta*, **46**, 1657 (2001).
21. T. Matsumoto, T. Komatsu, K. Arai, T. Yamazaki, M. Kijima, H. Shimizu, and Y. Nakamura, *Chem. Commun. (Cambridge)*, **2004**, 840.
22. K. H. Kangasniemi, D. A. Condit, and T. D. Jarvi, *J. Electrochem. Soc.*, **151**, E125 (2004).
23. R. L. Borup, J. R. Davey, F. H. Garzon, D. L. Wood, and M. A. Inbody, *J. Power Sources*, **163**, 76 (2006).
24. J. Wang, G. Yin, Y. Shao, S. Zhang, Z. Wang, and Y. Gao, *J. Power Sources*, **171**, 331 (2007).
25. C. N. R. Rao, B. Satishkumar, C. A. Govindaraj, and M. Nath, *ChemPhysChem*, **2**, 78 (2001).
26. K. P. De Jong and J. W. Geus, *Catal. Rev. - Sci. Eng.*, **42**, 481 (2000).
27. W. Li, C. Liang, W. Zhou, J. Qiu, Z. Zhou, G. Sun, and Q. Xin, *J. Phys. Chem. B*, **107**, 6292 (2003).
28. C. A. Bessel, K. Laubernds, N. M. Rodriguez, and R. T. K. Baker, *J. Phys. Chem. B*, **105**, 1115 (2001).
29. H. Wang, M. Chhowalla, N. Sano, S. Jia, and G. A. J. Amaratunga, *Nanotechnology*, **15**, 546 (2004).
30. J. N. Wang, Y. Z. Zhao, and J. J. Niu, *J. Mater. Chem.*, **17**, 2251 (2007).
31. H. Tamai, T. Sumi, and H. Yasuda, *J. Colloid Interface Sci.*, **177**, 325 (1996).
32. A. M. Kannan, V. P. Veedu, L. Munukutla, and M. N. G. Nejhad, *Electrochem. Solid-State Lett.*, **10**, B47 (2007).
33. E. P. Ambrosio, M. A. Dumitrescu, C. Francia, C. Gerbaldi, and P. Spinelli, *Fuel Cells*, **9**, 197 (2009).
34. Y. Huang, H. Cai, T. Yu, F. Zhang, F. Zhang, Y. Meng, G. Dong, Y. Wan, X. Sun, B. Tu, et al., *Angew. Chem., Int. Ed.*, **46**, 1089 (2007).
35. T. Ohkubo, J. Miyawaki, K. Kaneko, R. Ryoo, and N. A. Seaton, *J. Phys. Chem. B*, **106**, 6523 (2002).
36. D. Lee, J. Lee, J. Kim, J. Kim, H. B. Na, B. Kim, C. H. Shin, J. H. Kwak, A. Dohnalkova, J. W. Grate, et al., *Adv. Mater.*, **17**, 2828 (2005).
37. J. Lee, S. Yoon, T. Hyeon, S. M. Oh, and K. B. Kim, *Chem. Commun. (Cambridge)*, **1999**, 2177.
38. S. B. Yoon, J. Y. Kim, and J. S. Yu, *Chem. Commun. (Cambridge)*, **2001**, 559.
39. S. Yoon, J. Lee, T. Hyeon, and S. M. Oh, *J. Electrochem. Soc.*, **147**, 2507 (2000).
40. J. Lee, S. Yoon, S. M. Oh, C. H. Shin, and T. Hyeon, *Adv. Mater.*, **12**, 359 (2000).
41. H. S. Zhou, S. M. Zhu, M. Hibino, I. Honma, and M. Ichihara, *Adv. Mater.*, **15**, 2107 (2003).
42. F. B. Su, J. H. Zeng, X. Y. Bao, Y. S. Yu, J. Y. Lee, and X. S. Zhao, *Chem. Mater.*, **17**, 3960 (2005).
43. S. H. Joo, C. Pak, D. J. You, S. A. Lee, H. I. Lee, J. M. Kim, H. Chang, and D. Seung, *Electrochim. Acta*, **52**, 1618 (2006).
44. K. Wikander, H. Ekström, A. E. C. Palmqvist, A. Lundblad, K. Holmberg, and G. Lindbergh, *Fuel Cells*, **6**, 21 (2006).
45. X. Cui, L. Guo, F. Cui, Q. He, and J. Shi, *J. Phys. Chem. C*, **113**, 4134 (2009).
46. C. H. Christensen, I. Schmidt, A. Carlsson, K. Johannsen, and K. Herbst, *J. Am. Chem. Soc.*, **127**, 8098 (2005).
47. B. Fang, J. H. Kim, C. Lee, and J. S. Yu, *J. Phys. Chem. C*, **112**, 639 (2008).
48. P. Vinke, N. Van-tier-Eijk, M. Verbree, A. F. Voskamp, and H. Van-Bekkum, *Carbon*, **32**, 675 (1994).
49. V. Gómez-Serrano, F. Piriz-Almeida, C. J. Durán-Valle, and J. Pastor-Villegas, *Carbon*, **37**, 1517 (1999).
50. X. Chen, M. Farber, Y. Gao, I. Kulaots, E. M. Suuberg, and R. H. Hurt, *Carbon*, **41**, 1489 (2003).
51. H. I. Lee, S. H. Joo, J. H. Kim, D. J. You, J. M. Kim, J. N. Park, H. Chang, and C. Pak, *J. Mater. Chem.*, **19**, 5934 (2009).
52. B. K. Pradhan and N. K. Sandle, *Carbon*, **37**, 1323 (1999).
53. G. Inzelt, M. Pineri, J. W. Schultze, and M. A. Vorotyntsev, *Electrochim. Acta*, **45**, 2403 (2000).
54. C. Li, H. Bai, and G. Shi, *Chem. Soc. Rev.*, **38**, 2397 (2009).
55. W. J. Feast, J. Tsibouklis, K. L. Pouwer, L. Groenendaal, and E. W. Meijer, *Polymer*, **37**, 5017 (1996).
56. J. C. Chiang and A. G. MacDiarmid, *Synth. Met.*, **13**, 193 (1986).
57. L. F. Warren and D. P. Anderson, *J. Electrochem. Soc.*, **134**, 101 (1987).
58. Z. Qi and P. G. Pickup, *Chem. Commun. (Cambridge)*, **1998**, 2299.
59. B. Winther-Jensen, O. Winther-Jensen, M. Forsyth, and D. R. MacFarlane, *Science*, **321**, 671 (2008).
60. Y. S. Choi, S. H. Joo, S. A. Lee, D. J. You, H. Kim, C. Pak, H. Chang, and D. Seung, *Macromolecules*, **39**, 3275 (2006).
61. R. Bashyam and P. Zelenay, *Nature (London)*, **443**, 63 (2006).
62. R. Kiebooms, A. Aleshin, K. Hutchison, and F. Wudl, *J. Phys. Chem. B*, **101**, 11037 (1997).
63. G. Heywang and F. Jonas, *Adv. Mater.*, **4**, 116 (1992).
64. E. Antolini and E. R. Gonzalez, *Appl. Catal., A*, **365**, 1 (2009).
65. H. J. Ahonen, J. Lukkari, and J. Kankare, *Macromolecules*, **33**, 6787 (2000).
66. A. K. Sahu, K. G. Nishanth, G. Selvarani, P. Sridhar, S. Pitchumani, and A. K. Shukla, *Carbon*, **47**, 102 (2009).
67. J. Wang, X. Yu, Y. Li, and Q. Liu, *J. Phys. Chem. C*, **111**, 18073 (2007).
68. Y. Yang, Y. Jiang, J. Xu, and J. Yu, *Polymer*, **48**, 4459 (2007).
69. T. Soboleva, X. Zhao, K. Malek, Z. Xie, T. Navessin, and S. Holdcroft, *ACS Appl. Mater. Interfaces*, **2**, 375 (2010).
70. H. A. Gasteiger, S. S. Kocha, B. Sompalli, and F. T. Wagner, *Appl. Catal., B*, **56**, 9 (2005).
71. E. Ticianelli, C. R. Derouin, and S. Srinivasan, *J. Electroanal. Chem. Interfacial Electrochem.*, **251**, 275 (1988).
72. G. Selvarani, A. K. Sahu, N. A. Choudhury, P. Sridhar, S. Pitchumani, and A. K. Shukla, *Electrochim. Acta*, **52**, 4871 (2007).
73. B. Merzougui and S. Swathirajan, *J. Electrochem. Soc.*, **153**, A2220 (2006).